

## Theory of exciton spectra of incompressible quantum liquids

V. M. Apalkov

*Department of Physics, University of Utah, Salt Lake City, Utah 84112  
and L. D. Landau Institute for Theoretical Physics, Moscow 117940, Russia*

F. G. Pikus\*

*Department of Physics, University of Utah, Salt Lake City, Utah 84112*

E. I. Rashba

*Department of Physics, University of Utah, Salt Lake City, Utah 84112  
and L. D. Landau Institute for Theoretical Physics, Moscow 117940, Russia*

(Received 28 December 1994)

Energy and optical spectra of excitons against a background of incompressible quantum liquids (IQL's) are investigated by finite-size computations in a spherical geometry and by symmetry arguments based on the composite fermion theory. Properties of excitons are governed by the parameter  $h/l$ , where  $h$  is a separation between electron and hole confinement planes and  $l$  is a magnetic length. When  $h/l \lesssim 1$ , the energy spectrum comprises a single exciton branch  $L_0$  and a quasicontinuum above it. With increasing  $h/l$  a multiple-branch exciton spectrum develops. Different branches  $L_m$  may be classified by the index  $m$ , which identifies the minimum angular momentum,  $L_m$ , of the  $L_m$  branch. There are two types of branches. The branches of the first type are symmetrically compatible with a model of an exciton as a neutral entity consisting of a valence hole and several fractionally charged quasiparticles. All these anyon branches have  $m$  values exceeding some critical value ( $m \geq 3$  for the  $\nu = 1/3$  IQL), and they are generically related to some specific states from the low-energy sector of the electron subsystem, and drop down below the original  $L_0$  branch with increasing  $h/l$ . Comparative investigation of the number-of-particle dependencies of the electron and exciton spectra shows that these properties survive in the macroscopic limit and establishes a connection between anyon branches and the basic low-energy physics of IQL's. The branches of the second type remain above  $L_0$  and cannot be treated in terms of low-energy electronic excitations. We argue that the sphere-onto-plane projection rule for neutral composite particles has a form  $L - L_m = kR$ , where  $k$  is the particle quasimomentum and  $R$  is the sphere radius. Since a plane rather than a sphere is the dynamical space of an exciton, this projection rule clarifies the physical meaning of the multiple-branch spectra and establishes the selection rules for optical transitions. In particular, it identifies  $L_m$ 's as internal angular momenta of the excitons belonging to different branches. Momentum dependencies of the probabilities of magnetoroton-assisted transitions suggest that magnetorotons of a  $\nu = 1/3$ -IQL are  $L_2$  quasiparticles. We also show that doublet emission spectra originating from zero- and single-magnetoroton transitions persist in a wide region of the parameter values.

### I. INTRODUCTION

Incompressible quantum liquids (IQL's),<sup>1</sup> which are formed at low temperatures in a two-dimensional (2D) electron gas subjected to a strong magnetic field  $H$ , have been originally discovered by means of magnetotransport experiments. IQL's manifest themselves in the fractional quantum Hall effect (FQHE),<sup>2</sup> which is observed when a filling factor  $\nu$  takes quantized values  $\nu = p/q$  (in what follows, fractional fillings or fractions), where  $p$  is an integer, and  $q$  is an odd integer; for review, see Refs. 3 and 4. Intimate properties of these liquids, including the interaction of elementary excitations, are extracted from the theoretical treatment of the hierarchies,<sup>5-7</sup> i. e., families of IQL's. Members of these families manifest themselves consequently when the temperature  $T$  is lowered.

More recently optical experiments became an indepen-

dent source of information on the properties of IQL's. It is a specific property of interband optical experiments that the spectra are strongly affected by the electric field of a valence hole, a free or trapped one, which resides near the electron confinement layer. This field strongly complicates treatment of the data, but it also produces additional potentialities for investigating elementary excitations of IQL's. Meanwhile, the spectra of elementary excitations of IQL's are unique, and developing different approaches for the investigation of them seems highly tempting.

Charged elementary excitations of IQL's are quasidelectrons (QE's) and quasiholes (QH's) which are quasiparticles carrying fractional electric charges,  $(-e/q)$  and  $(e/q)$ , respectively. These quasiparticles are anyons, i. e., they obey fractional statistics.<sup>6,8</sup> Incompressibility of the liquids originates from the existence of a gap  $\Delta$  for creating a QE-QH pair. The lower branch of the spectrum of

neutral elementary excitations of an IQL is formed by magnetorotons (MR's).<sup>9</sup> A MR may be described either as a charge density wave,<sup>10</sup> or as a quasiexciton<sup>11</sup> consisting of a bound QE-QH pair. In the limit of a large momentum  $k$ , the MR frequency coincides with the gap,  $\omega_{\text{MR}}(k \rightarrow \infty) = \Delta$ .

There are three groups of successful experiments on optical properties of IQL's. The first group<sup>12</sup> deals with radiative recombination of electrons from a heterojunction with neutral acceptors residing outside the confinement layer. It is of crucial importance that the acceptors are neutral in the initial state and, therefore, do not perturb the IQL. As a result, the first moment of the emission band,  $\bar{\omega}(\nu)$ , shows down-cusps<sup>13</sup> at fractional fillings which are related to the cusps in the ground state energy.<sup>14</sup> However, cusp strengths in the emission spectra depend not only on  $\Delta$ , but also on the separation  $h$  between an acceptor and the electron confinement plane. Investigations of the  $\bar{\omega}(\nu)$  curves permitted experimentalists to observe the  $h$  dependence of the cusp strengths<sup>15</sup> and to measure the  $\Delta$  values for a number of IQL's.<sup>16</sup>

The second group of experiments deals with intrinsic recombination emission from quantum wells and heterojunctions. In the initial state a hole strongly polarizes an IQL, and magnetoexcitons having a complicated internal structure are formed. The most remarkable features in the intrinsic recombination spectra are doublets discovered in Ref. 17. This observation was supported by data taken by independent experimental groups.<sup>18,19</sup> Doublets were observed in the vicinity of fractional fillings, but they are also seen in a considerable region of  $\nu$  values around the fractions. In the region of small  $\nu$  values, which apparently corresponds to forming a Wigner solid, even more reach structures have been observed, and some theoretical approaches were discussed.<sup>20</sup> The patterns of the doublet spectra are somewhat different in quantum wells where up-cusps in the position of the high-frequency component have been found recently<sup>21</sup> (for a theory, see Ref. 22), and in heterojunctions with high<sup>18</sup> and low<sup>23,24</sup> electron concentrations. The origin of doublets has not been definitely established yet. In the vicinity of fractions the splitting of emission bands may originate from the presence of additional charged quasiparticles. A splitting mechanism originating from free QE's has been proposed in Ref. 25. A role of complexes, which are bound states of excitons with charged quasiparticles, has been mentioned in Refs. 26, 27. An extensive numerical investigation of such complexes, anyon ions,<sup>28,29</sup> has been performed in Ref. 30. Because of the inhomogeneity of samples (which is inevitable), complexes can contribute to emission spectra even when the  $\nu$  is nominally fractional. However, it has been shown<sup>31</sup> that there exists also a mechanism of the formation of doublets which operates when  $\nu$  takes a fractional value exactly. This mechanism is based on a gigantic suppression of the exciton dispersion by an IQL.<sup>26,32,33</sup> In the present paper we investigate this mechanism in more detail including the multiple-branch structure of exciton spectra.<sup>34</sup>

The third type of experiments<sup>35,36</sup> deals with resonant Raman scattering in the FQHE regime. These experiments permitted measuring the frequency of long-wave

MR's,  $\omega_{\text{MR}}(k = 0)$ , and the dispersion of MR's. Theories based on the band-to-band<sup>37</sup> and exciton<sup>38</sup> approaches have been proposed. Important aspects of the Raman scattering experiments, e.g., the spectral dependence of the scattering cross section, need a detailed description of the shape of exciton resonances.

One can see from the above summary that the central theoretical problem in the interband spectroscopy of the FQHE is the theory of excitons. The role of excitons in optical spectra increases with increasing magnetic field,<sup>39</sup> and they dominate the spectra of two-dimensional (2D) systems in the ordinary QHE regime.<sup>40-42</sup> Low-energy excitons remain stable also in the FQHE regime (despite the strong polarization of an IQL around them) because of the existence of the energy gap; numerical experiments<sup>26,30,32,33</sup> support this statement.

There are two parameters in the theory which strongly influence the properties of excitons. The first parameter is a 2D quasimomentum  $\mathbf{k}$ . It exists owing to the exciton electrical neutrality<sup>43</sup> and may be introduced by analogy with ordinary magnetoexcitons. The second parameter is the ratio  $h/l$ , where  $l$  is the magnetic length. It may be considered as a governing parameter which strongly influences both the internal structure and spectroscopy of excitons.<sup>44</sup>

When  $h = 0$ , (i) the perturbation exerted by a hole is large compared to  $\Delta$ , (ii) the size of an exciton is about  $l$ , which is the characteristic size of a QE, and (iii) electron concentration inside an exciton strongly deviates from the fractional value  $\nu/2\pi l^2$  (it reaches the Fermi limit,  $d_F = 1/2\pi l^2$ , at the point where a hole resides<sup>26</sup>). Therefore, one cannot expect that excitons might be described in terms of an unperturbed IQL, or, more specifically, of the elementary excitations of it. However, charge symmetric<sup>45</sup>  $h = 0$  systems possess a hidden symmetry. Owing to it frequencies of allowed exciton transitions exactly coincide with the transition frequencies in an empty crystal, i.e., in the absence of an IQL. This statement, established originally for Bose-condensed systems,<sup>40,46</sup> is valid under rather general conditions.<sup>32,33,47,48</sup> Computations in a spherical geometry<sup>5</sup> provide reliable results for small  $h$  values. However, the dynamic space of an exciton is a plane rather than a sphere. Therefore the conditions of a pseudoplane geometry,  $h \lesssim R/2$ , and of a small exciton radius,  $r_{\text{ex}} < \pi R$ , where  $R$  is the sphere radius, establish the upper limit for obtaining reliable quantitative results. The former restriction is practically equivalent to  $h/l \lesssim 1.5$ . Nevertheless, we believe that the qualitative results obtained in a spherical geometry remain valid for the lower part of the exciton spectrum in a wider region of  $h$  values,  $h \lesssim R$ , i.e.,  $h/l \lesssim 3$ .

The opposite limit case,  $h \gg l$ , is more accessible for an analytic treatment. In this limit the perturbation produced by a hole is weak as compared to  $\Delta$ , and an exciton consists of a valence hole with a charge ( $+e$ ) and  $q$  QE's having charges ( $-e/q$ ). Such an entity, an anyon exciton,<sup>29</sup> possesses a quasimomentum  $\mathbf{k}$  and  $(q - 1)$  internal degrees of freedom. As a result, the spectrum acquires a multiple-branch structure.<sup>29</sup> At  $k = 0$  the branches may be classified by the internal angular momentum of an exciton. With increasing  $k$  the electron

shell of an exciton shows impressive splitting into anyon components.<sup>49</sup> For  $q \gg 1$  the macroscopic approach<sup>22</sup> may be used.

In what follows, we report the results of computations in a spherical geometry<sup>5,50</sup> which show the emergence of the multiplicity of exciton branches from a wide continuumlike spectrum for  $\nu = 1/3$  (preliminary results were presented in Refs. 34). It is important that the multiple-branch spectrum sets in at  $h/l \approx 1.5$ , i.e., in the region of the applicability of the numerical methods. We believe that the latter property will permit one to match both approaches and to obtain the general picture of the spectrum dependence on  $h/l$ . Symmetry classification of the branches is given, and it is shown that the energy spectrum of excitons is intimately related to the dimension of the quasielectron space<sup>51</sup> and the decomposition of it into subspaces with different angular momenta.<sup>52,53</sup> Qualitative agreement with some predictions based on the anyon exciton model<sup>29,49</sup> is obtained.

## II. COMPUTATIONAL PROCEDURES

All computations have been performed in a spherical geometry.<sup>5,50</sup> Electrons and a hole were considered as particles inhabiting the lowest Landau level and possessing angular momentum  $S$ , where  $2S$  is the magnetic flux through the sphere in units of the flux quantum. The electron-hole separation  $h$  was modeled by the interaction Hamiltonian

$$H = \sum_{i < j} \frac{e^2}{R|\Omega_i - \Omega_j|} - \sum_i \frac{e^2}{\sqrt{h^2 + R^2|\Omega_i - \Omega_h|^2}}, \quad (1)$$

where  $R = l\sqrt{S}$  is the sphere radius,  $\Omega = \Omega(\theta, \phi)$  is a unit vector,  $i, j$  indicate electrons, and  $h$  denotes a hole. Following the usual procedure,<sup>50</sup> we have used Slater determinants as basis functions, computed Hamiltonian matrices for a given projection  $L_z$  of the angular momentum  $L$ , and found eigenvalues and eigenstates for  $L \geq L_z$ . The matrix size rises rapidly with the number of electrons  $N_e$  because of the increase in both the number of dynamical variables and the single-electron basis functions  $2S + 1$ . Adding a hole increases the size of the system by the factor about  $2S + 1$  because of the absence of antisymmetrization over the hole coordinate. For  $N_e = 8$  and a single hole,  $N_h = 1$ , the matrix size equals 42 164. Fortunately, the Hamiltonian matrix is sparse. The number of nonzero elements is only about 5%. Therefore, application of Lanczos<sup>54</sup> and Davidson<sup>55</sup> algorithms permitted us to find up to 50 lowest eigenvalues and their eigenfunctions for matrices of that size.

When evaluating the distribution of the electron density around the hole for an exciton with the angular momentum  $L$ , we have performed averaging over  $L_z$ . This averaged density  $d_L(\Omega)$  does not depend on  $\Omega_h$ . If one chooses  $\Omega_h = \Omega_h^0$  in the north pole direction, the following equation holds:

$$d_L(\theta) = \frac{4\pi}{Sl^2(2L+1)} \sum_{L_z} \int \cdots \int d\Omega_1 \cdots d\Omega_{N_e} \times |\Psi_{LL_z}(\Omega_1, \dots, \Omega_{N_e}, \Omega_h^0)|^2 \times \sum_i \delta(\Omega_i - \Omega_h^0 - \Omega). \quad (2)$$

The electron density on a hole, i.e., in the point where the hole resides, equals  $d_L(0)$  (more exactly, it is the electron density at the same point of the  $x, y$  plane). The Pauli exclusion principle determines the upper bound for  $d_L(\theta)$ ,

$$d_L(\theta) \leq d_F(S) = (2S+1)/4\pi Sl^2. \quad (3)$$

In the macroscopic limit,  $S \rightarrow \infty$ , this bound tends to  $d_F$ . The approximate density distribution in the plane geometry,  $d_L(r)$ , can be obtained by the chord projection

$$r = 2R \sin(\theta/2), \quad (4)$$

where  $\theta$  is the polar angle.

We suppose that interband transitions are allowed. In this case the photon angular momentum is absorbed by Bloch functions, and the probabilities and selection rules are determined by overlap of the electron and hole effective mass functions. Therefore the transition probabilities  $w_{if}$  in the emission spectra are equal to

$$w_{if} \propto \left| \int \cdots \int d\Omega_1 \cdots d\Omega_{N_e} d\Omega_h \Psi_i^*(\Omega_1, \dots, \Omega_{N_e}, \Omega_h) \times \Phi_f(\Omega_1, \dots, \Omega_{N_e-1}) \delta(\Omega_h - \Omega_{N_e}) \right|^2, \quad (5)$$

where  $\Psi_i$  and  $\Phi_f$  are the wave functions of the initial (with an exciton) and final (without exciton) quantum states. An analogous equation holds for absorption spectra.

## III. EXCITON STATES AT $h/l \leq 1$ : EXCITON BRANCH AND DOUBLET OPTICAL SPECTRA

In what follows we discuss the properties of a system with an exciton (or, what is the same, one additional electron-hole pair) and of the same system without the exciton. We shall refer to the former system as a “large” one and to the latter as a “small” one. To ensure reliability of the data we restrict  $L$  in the figures by the maximum MR angular momentum,  $(L_{MR})_{\max}$ ,<sup>9</sup> of a small system. For Laughlin liquids with  $\nu = 1/q$  this angular momentum equals  $(L_{MR})_{\max} = N_e^{(s)}$ , where  $N_e^{(s)} = N_e - 1$  is the number of electrons in a small system.

### A. Energy spectrum

The energy spectrum of a  $\nu = 1/3$  IQL with an exciton is plotted in Fig. 1 vs. angular momentum  $L$  for a system consisting of seven electrons and a single hole ( $N_e = 7$ ,  $N_h = 1$ ). Here and below energy is measured

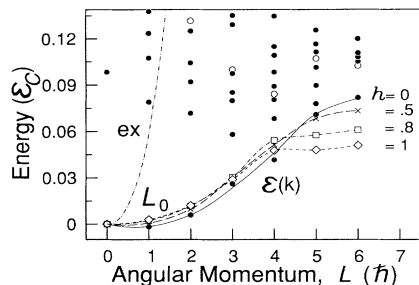


FIG. 1. Energy spectrum of a system consisting of seven electrons and one hole ( $N_e = 7, N_h = 1$ ) for  $h \leq 1$ . The flux  $2S = 15$ ; hence a small system is in an incompressible  $\nu = 1/3$  state. Maximum momentum of MR's is  $(L_{MR})_{\max} = N_e - 1 = 6$ . Since  $\varepsilon_0(L = 0)$  is chosen as the origin, multiplicative states display the MR dispersion law. For  $h = 0$  the exciton dispersion  $\varepsilon_0(L)$  and the continuum are shown. For different values of  $h$  only  $\varepsilon_0(L)$  is shown;  $h$  in units of  $l$ . For comparison the dispersion law of a bare exciton (ex) is shown;  $E_{\text{ex}}(k = 0)$  is chosen as the origin.

in units of the Coulomb energy  $\varepsilon_C = e^2/\epsilon l$ , while  $h$  and  $k$  are in units of  $l$  and  $l^{-1}$ , respectively;  $\epsilon$  is the dielectric constant. The spectrum includes a single exciton branch  $L_0$  and a quasicontinuum above it. For  $h = 0$  both the exciton dispersion law  $\varepsilon_0(k)$  and the continuum are shown in the figure;  $\varepsilon_0(0)$  is chosen as the origin. The lower branch of the multiplicative states<sup>26</sup> is shown by open dots. In these states two noninteracting quasi-particles are present: an  $L_0$  exciton with  $L = 0$  and a single MR. Therefore, open dots display the MR dispersion law. The roton minimum  $k_r$  is distinctly seen. If one employs the usual equation  $k = L/R$ ,<sup>4</sup> the magnitude of  $k_r$  is  $k_r \approx 1.5$ . It is also seen that some of the states belonging to the quasicontinuum lie below this minimum. We attribute them to complexes (exciton-MR bound states<sup>26</sup>), will not discuss them here in any detail, and will apply the term continuum to the whole spectrum lying above  $L_0$  and displaying no visible structure. The  $L_0$  branch and the continuum, well separated for  $k < k_r$ , draw together for  $k \gtrsim k_r$ . When  $h$  increases, the exciton energy  $\varepsilon_0(k)$  becomes flatter, and a gap opens between the  $L_0$  exciton branch and continuum. Meanwhile, there are no considerable changes in the distribution of the energy levels in the continuum.

The exciton dispersion law  $\varepsilon_0(k)$  is flat for  $k > k_r$ , and the exciton energy is strongly reduced in the whole area of  $k$  values because of the dressing of an exciton by an IQL. It is seen from Fig. 1 that  $\varepsilon_0(k)$  is about one order of magnitude smaller as compared to the energy of a bare exciton,  $E_{\text{ex}}(k = \infty) = \sqrt{\pi/2}$ . It seems plausible, by analogy with a quasiexciton,<sup>11,42</sup> that in the large  $k$  region,  $k \gg 1$ , an exciton consists of a core (an anyon ion), having a charge  $(e/q)$  [a hole and  $(q-1)$  QE's], and of a split-off QE. Calculations performed for anyon excitons with  $q = 2$  and  $3$  support this picture.<sup>29,49</sup> The separation between the core and the split-off QE in the large  $k$  region is about  $qk$ ; the energy is about  $\varepsilon_0(k) \approx \Delta/\varepsilon_C - 1/q^3$ . As applied to Fig. 1 this equation implies that  $\varepsilon_0(k)$  is

expected to increase by a factor of about 1.5 at  $k \rightarrow \infty$ . The shape and the scale of  $\varepsilon_0(k)$  are in reasonable agreement with the anyon exciton model.<sup>49</sup> These results imply that the charge fractionalization makes an essential contribution to the renormalization of the exciton energy spectrum and suppression of the exciton dispersion.

## B. Optical spectra

For  $h = 0$  the total oscillator strength is saturated by multiplicative states. Redistribution of it with increasing  $h$  is seen in Fig. 2. For  $h = 0$  multiplicative states are shown by bars. Quite analogous to Fig. 1, these states repeat the shape of the MR dispersion law. Because of the hidden symmetry (i) frequencies of the transitions to (from) multiplicative states do not depend on  $\nu$  (for  $\nu_e, \nu_h < 1$ ) and coincide with the exciton transition frequency in an empty crystal, and (ii) probabilities of the transitions to (from) all these states are equal. This latter fact is reflected in Fig. 2(a) in the equal lengths of all bars. In Figs. 2(b)–2(d) the probabilities are plotted in units of the length of these bars. When  $h$  increases, multiplicative states share the oscillator strength with different states of the continuum and of the  $L_0$  branch. Initially the oscillator strength is transferred to neighboring states [Fig. 2(b)], but later on the flow of the oscillator strength down the spectrum is clearly seen. This flow is especially

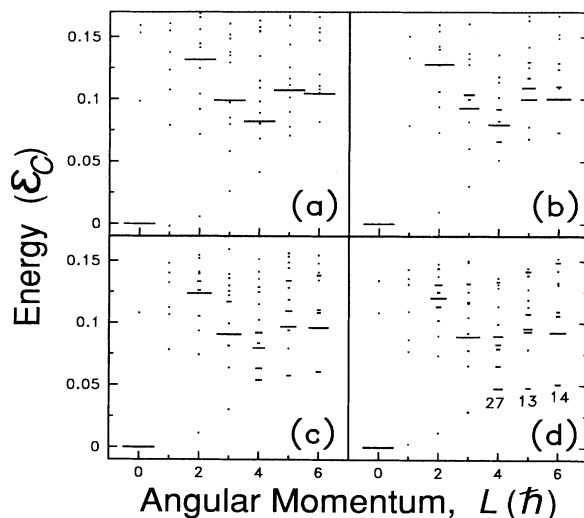


FIG. 2. Energy spectrum and distribution of the oscillator strengths between different states for four values of  $h$ : (a) 0, (b) 0.5, (c) 0.8, and (d) 1.0 ( $h$  in units of  $l$ ; bottom of the spectrum is chosen as the origin). The system is the same as in Fig. 1. (a) Multiplicative states which saturate the total oscillator strength are marked by bars. (b)–(d) Bar lengths show transition probabilities for zero-MR ( $L = 0$ ) and single-MR ( $L > 0$ ) transitions. In (d) the numbers show probabilities of single-MR transitions from the  $L_0$  branch in percentages of the transition probabilities from multiplicative states.

strong for  $k \gtrsim k_r$ . As a result, a considerable oscillator strength is accumulated near the bottom of the continuum and transferred to the exciton branch. For  $h = 1$  this latter part of the oscillator strength is rather high, Fig. 2(d).

The redistribution of the oscillator strength can also be displayed by the spectral function which includes both the transition probabilities and the density of states:

$$F(\omega) = \sum_{i\alpha} w_{i\alpha} \delta(\varepsilon_i - \varepsilon_\alpha - \omega), \quad (6)$$

where  $i$  and  $\alpha$ , respectively, refer to different states of “large” and a “small” system;  $w_{i\alpha}$  are transition probabilities.  $F(\omega)$  has a  $\delta$  function shape at  $h = 0$  and is picked at the frequency of a free magnetoexciton. In the left column of Fig. 3 the density  $F(\omega)$  is shown for three

values of  $h$ . Only the contribution to  $F(\omega)$  coming from the lower part of the energy spectrum, which is shown in Fig. 1, is included in Fig. 3; the upper part of the spectrum is immaterial for low- $T$  optical spectra, both emission and absorption. Three main contributions to  $F(\omega)$  are shown in the figure by different symbols. It is seen that the width of the spectral distribution increases with  $h$ . The contribution of the  $L = 0$  exciton state (heavy bars) is small due to a small phase volume, while the contribution of the  $L=4-6$  exciton states (full dots) is much larger owing to the high multiplicity,  $2L + 1$ , of these states.

Under the conditions of a quasiequilibrium, the emission spectrum is obtained by introducing into Eq. (6) the thermodynamic averaging over  $i$  states:

$$F_{\text{em}}(\omega) \propto \sum_{i\alpha} w_{i\alpha} \exp(-\varepsilon_i/T) \delta(\varepsilon_i - \varepsilon_\alpha - \omega). \quad (7)$$

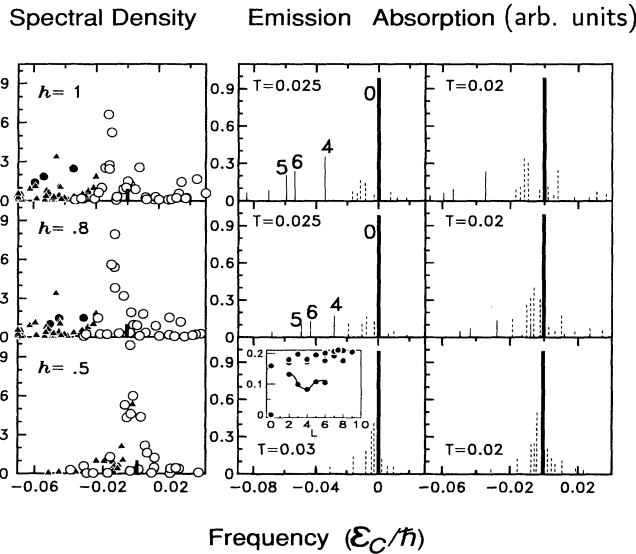


FIG. 3. Spectral density and emission and absorption spectra for three values of  $h \leq 1$ ; the system is the same as in Fig. 1. The value of  $h$  is constant in each row. The spectral density  $F(\omega)$  is shown in the left column. The  $L = 0$  zero-MR transitions and  $L \neq 0$  transitions between the  $L_0$  and MR branches are shown by bars and full dots, respectively. Only the states shown in Fig. 2 are included in  $F(\omega)$ ; the transitions involving high-energy states of the large system are of no significance for low- $T$  optical spectra. Transitions between the MR branch and the continuum of the large system are shown by open dots, and transitions between the  $L_0$  branch and non-MR states of the small system by triangles. Absorption and emission spectra:  $L = 0$  transitions and  $L \neq 0$  transitions between the  $L_0$  and MR branches are shown by heavy and light full lines, respectively, and transitions between the MR branch and the continuum of the large system by dashed lines. Angular momenta for strong transitions are shown by numbers. Heights of the lines show the intensities of the corresponding absorption and emission bands. Inset: energy spectrum of the small system,  $N_e^{(s)} = 6$ ; MR dispersion law is shown by a solid line (cf. Sec. VIB).  $h$ ,  $T$ , and  $L$  in units of  $l$ ,  $\varepsilon_C$ , and  $\hbar$ , respectively; frequency of the 0-0 exciton transition is chosen as the origin.

Low-temperature emission spectra calculated for three values of  $h$  are shown in the central column of Fig. 3. For understanding the properties of these spectra the following facts are of importance. (i) The energy of excitons is small along the  $\varepsilon_0(k)$  branch because of the strong suppression of the exciton dispersion, Sec. III A. Therefore all exciton states are populated at  $T$  as low as a few percent of  $\varepsilon_C$ . (ii) The dispersion law  $\varepsilon_0(k)$  is flat for  $k \sim k_r$ . Therefore the states with the energy about  $\varepsilon_0(k_r)$  have a large phase volume. (iii) The oscillator strength for single-MR transitions is large for  $k \sim k_r$ . (iv)  $\varepsilon_0(k) < \omega_r \equiv \omega_{\text{MR}}(k_r)$ ; hence, frequencies of single-MR-assisted transitions are lower than the frequency of the direct transition from the  $k = 0$  state.

The spectrum comprises only a single transition from the  $L = 0$  exciton state which is a direct transition to the ground state of the small system; transitions to different excited states of this system are very weak. For  $h = 0.5$  this peak is surrounded by transitions from different excited states which have borrowed the probability from multiplicative states and have nearly the same energies, cf. Fig. 2(b). When  $h$  increases, a new band emerges at the low-frequency side of the  $L = 0$  band. It originates from the transitions from the  $L_0$  branch to the MR branch, predominantly from the states with  $k \sim k_r$ , and is represented in Fig. 3 by emission lines 4–6. In the macroscopic limit these lines merge into a single band showing an Arrhenius type temperature dependence with the activation energy close to  $\varepsilon_0(k_r)$ . For  $h > 0.5$  this band is well separated from the  $L = 0$  band and its close satellites. Its total intensity is close to the intensity of the direct transition even at  $T$  as low as  $T = 0.025$  (in units of  $\varepsilon_C$ ). For  $h > 1$  the low-frequency band becomes stronger and even more isolated (see Fig. 4 below). We have proposed<sup>31</sup> that the upper components of the doublets observed by a number of workers originate from  $k = 0$  direct transitions while the lower components are their single-MR satellites, and have argued that there is a reasonable agreement between the theory and experimental data on the emission from quantum wells.<sup>17,35</sup>

Absorption spectrum may be found from the equation

$$F_{\text{ab}}(\omega) \propto \sum_{i\alpha} w_{i\alpha} \exp(-\varepsilon_\alpha/T) \delta(\varepsilon_i - \varepsilon_\alpha - \omega), \quad (8)$$

which differs from Eq. (7) only by averaging over the  $\alpha$  states of a small system. This spectrum is also shown in Fig. 3, right column. Since the magnetoroton branch (shown in the inset) is separated from the continuum, the transitions from this branch dominate in thermoactivated absorption. The  $L = 0$  transition from the ground state and transitions to those states in the continuum which originated from multiplicative states dominate in all absorption spectra shown in Fig. 3. These transitions fall in the same spectral region and should merge in a single band which may show a fine structure increasing with  $h$ . Low-frequency transitions to the exciton branch are weaker than corresponding transitions in the emission spectra. The pattern of the absorption spectrum can reveal itself also in the photoconductivity excitation spectra and the frequency dependence of the Raman cross section.

#### IV. EXCITON STATES AT $h/l > 1$ : NEW BRANCHES AND QUASIELECTRON SUBSPACES

It was shown in Sec. III that the energy spectrum consists of a single exciton branch  $L_0$  and a continuum for  $h \leq 1$ . We show in this section that the situation changes drastically for  $h > 1$ . New exciton branches split off from the continuum bottom. In what follows, we discuss the general patterns of the energy spectra and the manifestation of the multiplicity of exciton branches in the emission spectra. The origin of the different branches will be discussed in Sec. V.

##### A. Energy and emission spectra

In Figs. 4(a)–4(c) the energy spectrum is shown for a system of  $N_e = 7$  and  $N_h = 1$  for  $h \geq 1.6$ . Two new exciton branches which emerged from the bottom of the continuum and start at  $L = 1$  and 3 are seen in Fig. 4(a). The appearance of two more branches starting at  $L = 4$  and 5 can also be anticipated. The original  $L_0$  branch remains intact, but it becomes flatter as compared to Fig. 1. The value of the angular momentum each branch starts from,  $L_m$ , remains constant when  $h$  changes. Therefore, the  $L_m$ 's have the meaning of quantum numbers. They also will be used as labels for designating the branches.  $L_3$  and  $L_5$  branches move down fast and for  $h = 2.4$ , Fig. 4(b), they both pass below  $L_0$ .  $L_1$  and  $L_4$  branches remain above  $L_0$ , and  $L_2$  emerges above them. At  $h = 2.4$  a new branch,  $L_6$ , emerges; for  $h = 3$  it passes between  $L_5$  and  $L_0$ . In Fig. 4(c)  $L_6$  is represented by a single point because of a strong restriction imposed on  $L$  values,  $L \leq (L_{\text{MR}})_{\text{max}}$ . This branch is seen in Fig. 7 below where the energy spectrum is shown for a wider region of  $L$  values. It is remarkable that all branches which move down with increasing  $h$  and find themselves finally below  $L_0$  have  $L_m \geq 3$  ( $L_m \neq 4$ ), while the branches

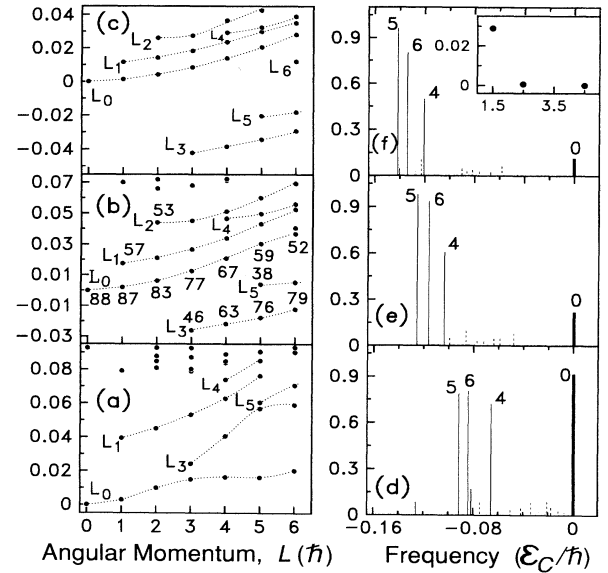


FIG. 4. Energy and emission spectra for three values of  $h \geq 1.6$  and  $T = 0.02$ ; the system is the same as in Fig. 1. On the left are energy spectra, on the right are emission spectra (arbitrary units).  $L_m$  indicate exciton branches. Numbers in (b) show electron density on a hole,  $d_L(0)$ , in percent of the Fermi limit,  $d_F(S)$ . In (d)–(f): solid lines represent exciton-MR transitions, dotted lines show exciton-continuum transitions; numbers show the angular momenta  $L$ . The electron-hole separation  $h$  is constant in each row: (a) and (d) 1.6, (b) and (e) 2.4, (c) and (f) 3.0;  $h$  in units of  $l$ . Inset of (f): low-energy sector for an  $N_e = 7$  system with 3 QE's. Energy in units of  $\varepsilon_C$ ; bottom of the  $L_0$  branch is chosen as the origin.

$L_m = 1, 2$ , and 4 remain above  $L_0$ . Investigating the dependence of the position of different points on  $h$ , which can be changed continuously, it is possible to check that the points connected by the curves drawn in Figs. 4(a)–4(c) move coherently and, therefore, belong to the same branch. The dependence of the probability of single-MR transitions on  $L$  along each branch is a different and very effective criterion, Sec. VI B. The picture becomes more complicated when some branch passes through another one. These events show patterns which are typical of avoided crossings of nearby branches. The assignment of points is most ambiguous near the continuum bottom, i.e., for the branches which are just originating from it.

The dependence of the emission spectra on  $h$  is shown in Figs. 4(d)–4(f) for a relatively low temperature  $T = 0.02$ . For  $h = 1.6$  the spectrum consists of two peaks. They are well separated, and the lower peak is stronger than the upper one because of the flattening of the  $\varepsilon_0(k)$  curve and a large phase volume for single-MR transitions. A critical change sets in at  $h \approx 2$  when  $L_3$  becomes the lowest branch of the spectrum. Under these conditions the lower peak originates from the single-MR transitions from the  $L_3$  branch; it dominates absolutely when  $T$  is low. This abrupt change in the emission has been pre-

dicted by two of us previously.<sup>26,31,33</sup> For the experimental observation of this abrupt change in the emission it is desirable to vary the ratio  $\hbar/l$  (e.g., by changing  $l$ ) under the conditions of  $\nu=\text{const}$ .<sup>44</sup>

Single-MR satellites dominate the spectrum of indirect transitions, i.e., the transitions assisted by creation of neutral excitations. The probabilities of these transitions strongly depend on  $L$  for most of the branches; the origin of this dependence will be discussed in Sec. VIB. The probabilities depend also on  $\hbar$  and  $L_m$ . However, for some branches two-MR transitions are rather strong. For example, for the  $L_6$  branch the transition probabilities to the states having energies about  $2\omega_{\text{MR}}(k_r)$  reach about 5% of the transition probability from multiplicative states.

### B. Finite widths of confinement layers and polarizability effects

The previous computations were performed for ideal 2D systems with infinitely narrow electron and hole confinement layers. In this section we consider layers having finite widths to check whether the qualitative results obtained above are robust, and how the properties of real systems differ from the properties of the ideal ones. For this purpose we use the effective electron-electron<sup>56</sup> and electron-hole interactions:

$$V_{ee}(\Omega_1, \Omega_2) = \int_0^\infty dz_1 \int_0^\infty dz_2 \frac{|\zeta_e(z_1)|^2 |\zeta_e(z_2)|^2}{[R^2(\Omega_1 - \Omega_2)^2 + (z_1 - z_2)^2]^{1/2}}, \quad (9)$$

$$V_{eh}(\Omega_1, \Omega_h) = - \int_0^\infty dz_1 \int_0^\infty dz_2 \frac{|\zeta_e(z_1)|^2 |\zeta_h(z_2)|^2}{[R^2(\Omega_1 - \Omega_2)^2 + (\hbar - z_1 - z_2)^2]^{1/2}}, \quad (10)$$

where  $\zeta_e(z)$  and  $\zeta_h(z)$  are  $z$ -dependent wave functions of the Fang-Howard type<sup>57</sup>

$$\zeta_e(z) = (b_e^3/2)^{1/2} z \exp(-b_e z/2), \quad (11)$$

$$\zeta_h(z) = (b_h^3/2)^{1/2} z \exp(-b_h z/2).$$

The results of computations for a system consisting of a six-electron  $\nu = 1/3$  IQL and a single exciton are shown in Fig. 5 for  $b_h^{-1} = 0.4$  and  $b_e^{-1} = 0.2$ . It is seen that the data are similar to those for ideal systems but with reduced  $\hbar$  values. This reduction is caused by the fact that the distance between the maxima of the electron and hole densities, which plays the role of an effective  $\hbar$ , is less than the geometric  $\hbar$ ; cf. the inset of Fig. 5(g).

Therefore the main properties of ideal systems such as a multiple-branch energy spectrum and a two-peak emission spectrum are robust. It is the main difference of the

finite-width 2D layers from the ideal ones that similar energy spectra appear at somewhat larger  $\hbar$  values. The inset of Fig. 5(g), where the electron and hole density distributions in the  $z$  direction are shown, clarifies this conclusion. Indeed, for finite-width 2D layers the effective electron-hole separation in the  $z$  direction is smaller than for an ideal system of the same total width.

The above finite-width model does not take into account the particle dynamics in the  $z$  direction which may turn out to be very important. Because the effective potential for a hole is much flatter than for electrons, the main effect is expected to come from the hole polarizability.

From the above results for ideal systems, Fig. 4(b), it is seen that the electron density on a hole,  $d_L(0)$ , depends on the spectrum branch and on  $L$ . A convenient unit of the density is the Fermi limit  $d_F(S)$ , cf. Sec. II. For

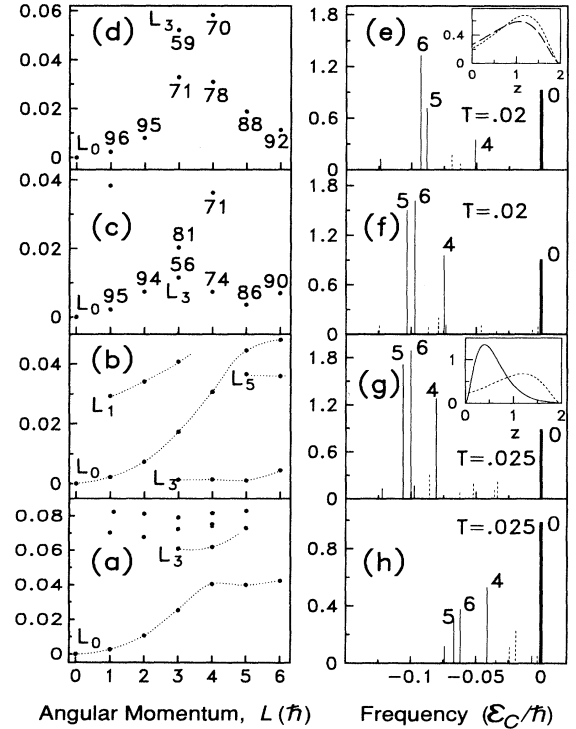


FIG. 5. Energy and emission spectra of a system with finite electron and hole confinement layers widths.  $N_e = 7, N_h = 1$ , flux  $2S = 15$ , a small system is in an incompressible  $\nu = 1/3$  state. On the left are energy spectra; on the right are emission spectra (arbitrary units). The separation  $\hbar$  in units of  $l$  is constant in each row: 1.5 for (a), 2.0 for (b)–(d);  $\hbar$  in units of  $l$ . Confinement layer parameter values are  $b_e^{-1} = 0.2l, b_h^{-1} = 0.4l$ . Polarizability  $\alpha = 0$  for two lower rows; it is equal to  $\alpha = 0.02$  for (c) and (f) and to  $\alpha = 0.1$  for (d) and (e) ( $\alpha$  in units of  $l$ ). Numbers in (c) and (d) show  $d_L(0)$  in percent of  $d_F(S)$ . Inset of (g): electron (solid line) and hole (dotted line)  $z$  distribution for  $L = 0, \alpha = 0$ . Inset of (e):  $z$  distribution of the hole density for  $L = 0; \alpha = 0$  (dotted line),  $\alpha = 0.1$  (dashed line),  $z$  in units of  $l$ . Energy and  $T$  in units of  $\epsilon_C$ ; bottom of the  $L_0$  branch is chosen as the origin.

example, for the  $L_0$  branch the density  $d_0(0)$  is close to  $d_F(S)$ , while for the  $L_3$  branch it is about  $0.6d_F(S)$ . It is natural to expect that the larger  $d_L(0)$  is, the larger the attracting force acting on the hole in the  $z$  direction also is. As a result, in a system with a distributed hole density the hole should approach the electron confinement layer. The above discussion suggests a model which takes into account the  $z$  dynamics of a hole by renormalization of  $b_h$ . For a state with a given  $d_L(0)$ , the effective width of the hole confinement layer is

$$b_h^{-1}[d_L(0), \alpha] = b_h^{-1} + \alpha[d_L(0)/d_F(S) - \nu], \quad (12)$$

where the coefficient  $\alpha$  has the meaning of the hole polarizability.

To evaluate the effect of the hole polarizability, we have solved the problem in a linear approximation in  $\alpha$ . It is seen from Figs. 5(c) and 5(d) that the exciton energy spectrum is highly sensitive to the polarizability effect even for rather small values of  $\alpha$ . For  $L \geq 3$  there are two branches, the rising and the descending ones. In this area of the  $L$  values the assignment of the branches as  $L_0$  and  $L_3$  is rather conditional. For  $\alpha = 0.02$  [Fig. 5(c)] the lower branch possesses lesser values of  $d_L(0)$  and may be assigned as  $L_3$ , while for  $\alpha = 0.1$  the  $L_3$  assignment seems to be more appropriate for the upper branch. It is remarkable that these drastic changes in the dispersion law are caused by minor changes in the hole density distribution as seen from the inset of Fig. 5(e). The emission spectrum is less sensitive to the  $\alpha$  values than the energy spectrum, and it retains the doublet shape as seen from Figs. 5(e) and 5(f).

## V. ORIGIN OF THE MULTIPLE-BRANCH SPECTRA

In this section we discuss the origin of the multiple-branch exciton spectra described in Sec. IV and establish the interrelation existing between these spectra and the low-energy physics of the FQHE, i.e., with elementary excitations of an IQL in the absence of a valence hole. The multiple-branch spectra of Sec. IV have been obtained by computations in a spherical geometry which have two obvious limitations. First, the finite area of a sphere results in a size quantization. We show that the multiplicity of the exciton branches is not an artifact of the size effect and establish the quantum numbers of the branches which survive in the continuum limit. Moreover, we argue that exciton branches can be divided into two groups, and that one of the groups is closely related to the Hilbert space of QE's,<sup>51</sup> and, in particular, to the decomposition of it into subspaces with different angular momenta.<sup>52,53</sup> The hole works as a probe which explores the internal structure of the QE space. The second limitation is related to the criterion of the pseudoplane geometry,  $h \ll R$ . To receive reliable results, we have performed all computations under the conditions  $h \lesssim R$ , and have checked the spatial extension of the exciton wave functions.

Multiple-branch exciton spectra have been obtained

originally in the framework of the anyon exciton model.<sup>29,49</sup> The spectra described in Sec. IV, and the relation between the exciton branches and the spectrum of the electronic subsystem in the absence of a hole which will be discussed in this section corroborate our belief that the anyon exciton approach provides a correct description in the  $h \gg 1$  region (the  $h \rightarrow \infty$  limit corresponds to free QE's<sup>25</sup>). In this connection we survey here some properties of anyon excitons which will be of importance for us in what follows. Their energy spectrum is described by two quantum numbers, the angular momentum  $\mathcal{M} \leq 0$  which enumerates the branches and the quasimomentum  $\mathbf{k}$ . In the large  $h$  region, the spatial size  $R_b$  of the state which forms the spectrum bottom increases with  $h$  as  $R_b \propto h$ , while the angular momentum of this state increases as  $|\mathcal{M}_b| \propto h^2$ . The difference in successive values of  $\mathcal{M}_b$  equals 3 for a three-anyon exciton.

### A. $L_m$ as quantum numbers

Examination of Figs. 4(a)–4(c) shows that the starting point,  $L_m$ , of each branch remains unchanged since the instant when the branch can be definitely recognized.  $L_m$  is preserved at the movement of the branch, branch crossings, etc. This fact implies that  $L_m$  is a quantum number. A comparison of Figs. 4(a)–4(c) with Fig. 6

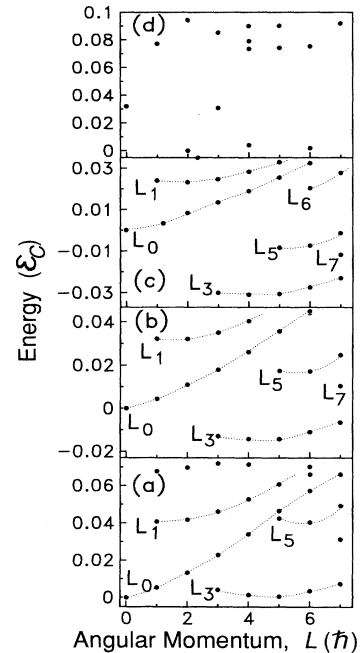


FIG. 6. Energy spectrum of a system of a seven-electron  $\nu=1/3$  IQL and an exciton; bottom of the  $L_0$  branch is chosen as the origin.  $N_e = 8$ ,  $N_h = 1$ , flux  $2S = 18$ . Maximum angular momentum of MR's is  $(L_{MR})_{\max} = N_e - 1 = 7$  in the incompressible state of the small system. The separation  $h = 2.0$  (a), 2.4 (b), and 3.0 (c) (in units of  $l$ ). In (d) the energy spectrum is shown for an  $N_e = 8$  system with 3 QE's (it is in agreement with the data of Ref. 52).

obtained for the same  $\nu = 1/3$  IQL, but for the larger number of electrons  $N_e = 8$ , establishes the even more important facts that the values of  $L_m$ 's do not depend of the system size, and the order in which the branches appear is nearly independent of  $N_e$ . Indeed, the main patterns of Figs. 4(a)–4(c) and Fig. 6 are the same. The original branch  $L_0$  is followed by  $L_1$  and  $L_3$ , then  $L_3$  is followed by  $L_5$  and  $L_6$  (for  $N_e = 8$  also the  $L_7$  branch appears); the branches  $L_3$ ,  $L_5$ , and  $L_6$  move down with increasing  $h$ , while  $L_1$  remains above  $L_0$ , etc. Systems with  $N_e = 5$  and 6 show analogous properties. These facts suggest that the quantum numbers  $L_m$  survive in the macroscopic limit,  $N_e \rightarrow \infty$ .

### B. {QE} $h$ coupling scheme

Everywhere above we have plotted exciton dispersion curves  $\varepsilon_m(L)$  only inside a “narrow window,” for  $L \leq (L_{MR})_{\max}$ , since the data for energy spectra are most reliable in this region of  $L$  values. For  $L > (L_{MR})_{\max}$  the  $\varepsilon_m(L)$  curves rise steeply rather than saturate, as physical arguments and the anyon exciton model<sup>29,49</sup> suggest. However, some regularities related to the systematics and counting the states become more evident when seen through a “broad window.” In Fig. 7 the data are shown for the same system as in Figs. 1 and 4(a)–4(c), but for  $L \leq 12$ . The data for the three lower branches ( $L_3$ ,  $L_5$ , and  $L_6$ ) can be described by the usual rule of the addition of the electron and hole angular momenta,  $L_e$  and  $L_h$ :

$$D(L_e) \otimes D(L_h) = D(L_h - L_e) \oplus \cdots \oplus D(L_h + L_e), \quad (13)$$

if one takes into account the low-energy spectrum of an  $N_e = 7$  electron system which is shown in the inset of Fig. 4(f). Its angular momentum decomposition ( $L_e$  decomposition) includes three subspaces with  $L_e = 4.5$ , 2.5, and 1.5. Since  $2S = 15$ , the angular momentum of the hole equals  $L_h = 7.5$ , and the three sequences determined

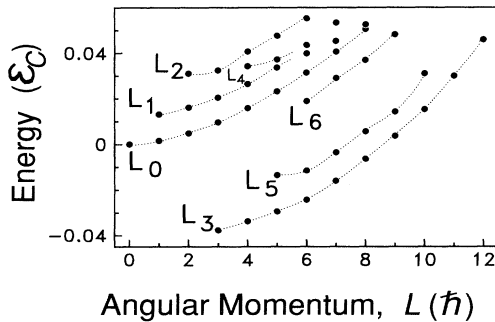


FIG. 7. Energy spectrum in a wide region of  $L$  values; energy of the  $L_0(L = 0)$  state is chosen as the origin. The system is the same as in Figs. 1 and 4;  $h = 2.8$  (in units of  $l$ ). The number of states on  $L_3$ ,  $L_5$ , and  $L_6$  branches is in agreement with the {QE} $h$  coupling scheme, Eq. (13).

by Eq. (13) are  $D(3) \oplus \cdots \oplus D(12)$ ,  $D(5) \oplus \cdots \oplus D(10)$ , and  $D(6) \oplus \cdots \oplus D(9)$ . They correspond exactly to the three branches,  $L_3$ ,  $L_5$ , and  $L_6$ , seen in Fig. 7 below  $L_0$ . Figure 7 suggests the existence of a one-to-one correspondence between the energy spectrum of excitons and the  $L_e$  decomposition of the low-energy spectrum of the electron system (in the absence of a hole), and shows that the angular momentum coupling scheme which can be termed a {QE} $h$  coupling, operates. It describes the interaction of the total angular momentum of three QE's, which equals  $L_e$ , with the momentum of a hole,  $L_h$ . The applicability of this scheme seems obvious in the perturbation theory region,  $h \gg R$ , since according to Eq. (1) the electron-hole interaction decreases as  $h^{-1}$  and is small as compared to the interaction of QE's which is restricted by  $R^{-1}$ . However, this region is unphysical since in a real geometry the mean separation between QE's is scaled by  $h$  for  $h \gg 1$ ; hence, it cannot be described in the spherical geometry. The data of Fig. 7 are shown for  $h = 2.8$  when the QE-hole interaction is strong. It is comparable to the inter-QE interaction, and the  $L_3$  and  $L_5$  branches show the same patterns up to  $h \approx 2$ . Under these conditions the origin of the {QE} $h$  coupling for a four-particle system, three QE's and a single hole, is not obvious. Apparently, this coupling is tantamount to the existence of well separated anyon branches, and it should be treated in terms of the counting-of-states arguments.

It follows from Eq. (13) that the minimum angular momentum of an exciton equals  $L_m = L_h - L_e$  for each exciton branch. When  $N_e$  increases, both  $L_h$  and  $L_e$  also increase. The independence of  $L_m$  of the system size, which has been established in Sec. V A, shows that the  $N_e$  dependencies of  $L_h$  and  $L_e$  cancel. As applied to the  $L_3$  branch, the origin of this cancellation will be established in Sec. V C.

Therefore the exciton spectrum consists of two groups of branches. The branches  $L_3$ ,  $L_5$ , etc. are related to the electronic  $L_e$  subspaces of the low-energy sector. The  $L_0$  branch and the branches which remain above it when  $h$  increases are of different nature.

### C. Critical exciton branch and macroscopic limit

The data of Figs. 4(a)–4(c), 6, and 7 show that all branches  $L_m$  which drop down with increasing  $h$  and find themselves finally below  $L_0$  have  $m \geq 3$ ; hence,  $L_3$  is a critical branch. It is typical of anyon excitons<sup>29,49</sup> that with increasing  $h$  the branches with large angular momenta  $|M|$  drop down and reach the spectrum bottom. Therefore it is necessary to establish what are the restrictions on  $L_m$  which are imposed (in a spherical geometry) by the requirement that the  $L_m$  exciton consists of  $q$  QE's and a hole.

The maximum angular momentum of several QE's may be found by applying the composite fermion theory<sup>7</sup> to a Laughlin liquid with  $\nu = 1/q$ . A system consisting of  $N_e$  electrons and  $q$  QE's is represented in this theory by the ground Landau level of a Jain's sphere filled by a  $\nu = 1$  phase of  $(N_e - q)$  electrons and the next Landau

level populated by  $q$  electrons.<sup>58</sup> Therefore the flux equals  $2S_J = N_e - q - 1$ . Each of the electrons of the second Landau level possesses the angular momentum  $S_J + 1$ , and since electrons are subject to the Pauli exclusion principle, the maximum projection  $(L_{QE})_z$  of the total angular momentum is  $(L_{QE})_z = q(S_J + 1) - q(q - 1)/2$ . Substituting the value of  $S_J$ , one finds the maximum angular momentum of  $q$  QE's which coincides with  $(L_{QE})_z$ . It is

$$(L_{QE})_{\max} = qN_e/2 - q(q - 1). \quad (14)$$

In the presence of  $q$  QE's the flux through the Haldane's sphere is  $2S = \nu^{-1}(N_e - 1) - q$ , and the angular momentum of the hole is

$$L_h = S = qN_e/2 - q. \quad (15)$$

Therefore  $L_h > (L_{QE})_{\max}$ , and the minimum angular momentum of an exciton which may be achieved in the framework of the QE-hole model is

$$(L_{ex})_{\min} = L_h - (L_{QE})_{\max} = q(q - 2). \quad (16)$$

This equation includes the magnitude of the *maximum angular momentum of  $q$  QE's* and, therefore, is not based on the  $\{QE\}h$  coupling scheme. For  $q = 3$

$$(L_{ex})_{\min} = 3. \quad (17)$$

This is just the critical momentum  $L_3$  found by computations. The results of Sec. VB and the above result imply that both the  $\{QE\}h$  coupling scheme and the composite fermion theory select the same group of the branches for excitons which are *symmetrically compatible* with a picture of composites consisting of a hole and  $q$  QE's. In this sense we shall term these branches *anyon branches*. Excitons belonging to different branches like  $L_0, L_1$ , etc. will be termed *tight excitons*. They are built of the electron states of the high-energy sector, but can also include some contribution from the states of the low-energy sector; this contribution can depend on  $h$  and  $L$ .

An exciton having  $L_m = (L_{ex})_{\min}$  possesses the maximum density of the electron cloud in the vicinity of the hole which is attainable for anyon branches. Indeed, for  $(L_{QE})_z = (L_{QE})_{\max}$  the fermion orbits on the second Landau level of the composite fermion construction have the maximum projections on the  $z$  axis and therefore produce a narrow electron density distribution near the north pole of the sphere. The condition  $L = L_m$  (which is analogous to  $\mathbf{k} = \mathbf{0}$  in the plane geometry, cf. Sec. VIA) ensures that the hole density is peaked in the same area.

It is seen from Eqs. (14)-(16) that  $N_e$  cancels out from  $(L_{ex})_{\min}$ , which proves that  $(L_{ex})_{\min}$  retains its meaning in the macroscopic limit. The analytic derivation performed here for the critical branch supports the computational results of Sec. VB.

Side by side with the critical branch  $L_3$ , several next anyon branches are of special interest. They originate from the QE states having angular momenta less than  $(L_{QE})_{\max}$  but close to it. A comparison of the inset to Fig. 4(f) with Fig. 6(d) reveals a striking analogy in the configurations of the three points constituting the low-

energy sector for  $N_e = 7$ , Fig. 4(f), and of the three right-hand points of the low-energy sector for  $N_e = 8$ , Fig. 6(d). The general shift in  $L_e$  is immaterial since for excitons it cancels with the shift in  $L_h$ . In both cases the state with  $L_m = (L_{QE})_{\max} - 1$  is absent, the states  $(L_{QE})_{\max}$  and  $(L_{QE})_{\max} - 2$  have nearly the same energies, and the energy of the  $(L_{QE})_{\max} - 3$  state is larger than them by an amount which is somewhat less than 0.03. The absence of the  $L_m = (L_{QE})_{\max} - 1$  state is not accidental. It follows from the fermionic behavior of QE's in the composite fermion theory. Indeed, there is only a single Slater determinant with  $(L_e)_z = (L_{QE})_{\max} - 1$  which obviously belongs to the momentum  $(L_{QE})_{\max}$ . The fact that the configuration of the right-hand states is stable and only weakly depends on  $N_e$  is confirmed by the data of Fig. 8(a) for an  $N_e = 9$  system. It is seen that the low-energy sector is well separated from the upper part of the spectrum, and considerable changes occur only in the left-hand side of this sector when  $N_e$  increases. In particular, for the first time there appears a state,  $(L_{QE})_{\max} - 5$ , which has an energy which is noticeably lower than the energy of the tight QE complex having the momentum  $(L_{QE})_{\max}$ . The energy difference of the states  $(L_{QE})_{\max}$  and  $(L_{QE})_{\max} - 3$  changes by about 25% when  $N_e$  increases from  $N_e = 7$  to  $N_e = 9$ . In general,

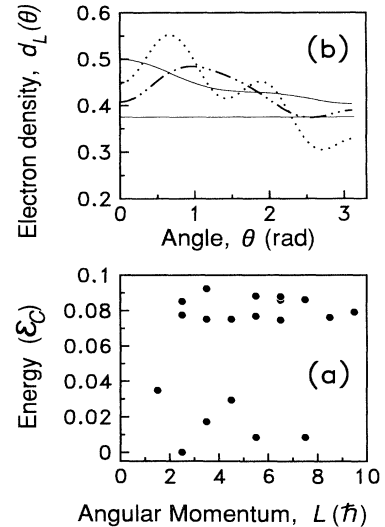


FIG. 8. Properties of many-electron systems in the absence of a hole. (a) Energy spectrum of a  $\nu = 1/3$  system of  $N_e = 9$  electrons and 3 QE's; energy of the ground state is chosen as the origin. The right-hand side of the low-energy sector nearly repeats the spectrum of Fig. 4(f) (inset) and the same part of the spectrum of Fig. 6(d). (b) Electron density distribution for three-QE states of the low-energy sector for  $L_z = L$ ;  $N_e = 7$ . The density  $d_L(\theta)$  in units of  $d_F(S)$  is plotted vs polar angle  $\theta$ ;  $L = 4.5$  (dotted line), 2.5 (dash-dotted line), and 1.5 (solid line). Horizontal line shows the density of the  $\nu = 1/3$  IQL. Positions of the corresponding energy levels are shown in the inset of Fig. 4(f). The density becomes smoother with increasing  $(L_{QE})_{\max} - L$ ;  $(L_{QE})_{\max} = 4.5$ .

increase in  $N_e$  results in developing the low-momentum part of the low-energy sector. The weak dependence of the high-momentum electron states on  $N_e$  originates from the fact that they are relatively small three-QE complexes scaled by the magnetic length, Fig. 8(b). Their size is the smaller the less the difference  $(L_{QE})_{\max} - L$  is. These complexes constitute a discrete sequence, and their energies tend to finite values in the macroscopic limit,  $N_e \rightarrow \infty$ . A considerable spread of the electron density of the  $L_{QE} = 1.5$  state which is comparable to the system size  $\pi R$ , can explain the aforementioned 25% size shift in its energy level. It is more difficult to understand why the two tightest three-QE complexes with the momenta  $(L_{QE})_{\max}$  and  $(L_{QE})_{\max} - 2$  have low energies (low energies of some large  $L_{QE}$  complexes are in accordance with the data of Ref. 52). This fact, at least partially, may be attributed to the suppression of the low- $L$  two-QE quasipotentials as compared to their Coulomb values found in Ref. 59, and apparently implies the existence of a three-QE attractive short range interaction; it needs special consideration.

There is a remarkable analogy between the electron densities in the  $L_{QE} = 4.5$  and  $2.5$  three-QE complexes, Fig. 8(b), and the electron densities in  $L_3$  and  $L_5$  excitons, Fig. 9(d), which originated from these electron subspaces. Independence of the electron density on  $h$  is typical of  $k = 0$  states of anyon excitons with low momenta  $\mathcal{M}$ .<sup>49</sup>

Since anyon branches originate from specific three-QE complexes, Sec. V B, exciton energies depend on the energies and spatial sizes of these complexes. The low energy of the three-QE complex and the small size of it (which increases the QE-hole attraction) result in a low exciton energy in the region of moderate  $h$  values,  $h \approx 2$ . These arguments, in conjunction with the data of Figs. 4(f), 6(d), and 8, explain clearly why the  $L_3$  branch is the first to appear and why the  $L_4$  branch is absent from the lower part of the spectrum. The latter only appears near the bottom of the continuum, Figs. 4(c) and 7. The mutual position of the  $L_5$  and  $L_7$  branches (the latter appears in Fig. 6) is not clear yet because of the considerable difference in the energies of the  $(L_{QE})_{\max} - 4$  state in Figs. 6(d) and 8(a) caused by the size effect.

It follows from the above arguments that for  $h \approx 2$ , when the  $L_3$  branch and a couple of branches following it are close to the spectrum bottom, their energies are determined by the interaction of QE's and a hole at the spatial scale of a few magnetic lengths. Therefore, *energies of these excitons obtained in the spherical geometry should be valid in the macroscopic limit*. All these data for exciton spectra are closely related to the energy spectrum of the electron subsystem. For intermediate  $h$  values some low-lying three-QE states with a considerable difference  $(L_{QE})_{\max} - L$ , like the  $(L_{QE})_{\max} - 5$  state in Fig. 8(a), can show up near the exciton spectrum bottom. In the region of large  $h$  values, the states  $L_m$  with  $m \gg 1$  move down and approach the spectrum bottom, mean distances between QE's increase, and the deviation of the QE interaction from a Coulomb law diminishes. In this limit the anyon exciton approach<sup>29,49</sup> or the macroscopic description<sup>22</sup> are expected to become preferable.

#### D. Electron density distribution

It has been shown in Secs. V B and V C that there exist two different groups of exciton branches. The distribution of the electron density inside excitons gives more insight onto the origin of both types of excitons.

In Fig. 9(a) the electron density distribution  $d_L(r)$  for an  $L_3$  exciton is shown for the starting point of the

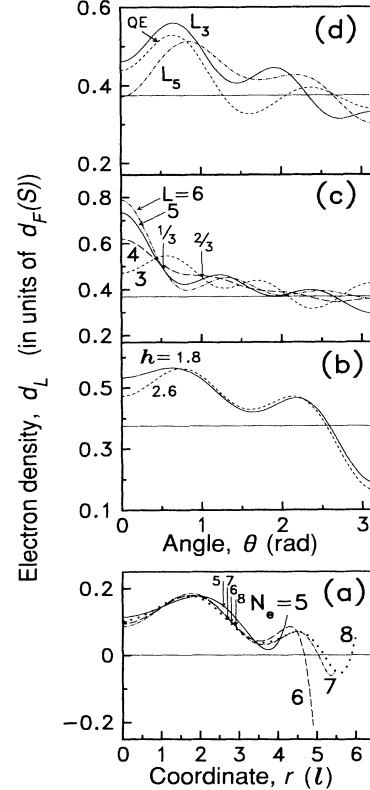


FIG. 9. Electron density distribution for  $L_3$  and  $L_5$  excitons. All curves were obtained by averaging over the projections  $L_z$  of the exciton angular momentum. (a) Density distribution  $d_3(r)$  for an  $L_3$  exciton plotted vs coordinate  $r$  for  $L = 3$ ,  $h = 2.6$ . The electron-hole separation  $r$  is chosen along a chord, Eq. (4). Different curves describe the systems with  $5 \leq N_e \leq 8$ . Arrows show the boundaries of the areas where  $2/3$  of the electron charge is accumulated. The second maximum may be attributed to a split-off QE. The density of a  $\nu = 1/3$  IQL is chosen as the origin. (b) Dependence of the density distribution  $d_3(\theta)$  on  $h$  for an  $L_3$  exciton. The hole resides at the north pole;  $N_e = 7$ . (c) Dependence of  $d_L(\theta)$  on the exciton angular momentum,  $L \geq 3$ , for an  $L_3$  exciton;  $h = 2.6$ ,  $N_e = 7$ . The boundaries of the areas where charges  $1/3$  (for  $L = 6$ ) and  $2/3$  (for  $L = 3$ ) are accumulated are shown by arrows. (d) Density distributions  $d_L(\theta)$  for  $L_3$  and  $L_5$  excitons (for the momenta  $L = 3$  and  $L = 5$ , respectively);  $h = 2.6$ ,  $N_e = 7$ . The density distribution for a single QE is shown for comparison;  $L_z = L = N_e^2/2 = 3$  (it is in agreement with the data of Ref. 9).  $h$  in units of  $l$ ,  $L$  in units of  $\hbar$ . In (b)–(d) the density of the  $\nu = 1/3$  IQL is shown by horizontal lines.

branch,  $L = 3$ . The calculations were performed for systems of  $5 \leq N_e \leq 8$  electrons, and the results are plotted versus the coordinate  $r$ . It is seen that the size of the exciton is about several magnetic lengths, and  $d_L(r)$  deviates from its value in a homogeneous  $\nu = 1/3$  IQL over the whole sphere. There are seen two distinct maxima in the density. The shape of the first maximum is well defined even for  $N_e = 5$ , while in the area of the second maximum the density distribution converges only for large systems,  $N_e \geq 7$ . The boundary of the region where  $2/3$  of the electron charge is accumulated is shown by an arrow on each curve. The position of this boundary only weakly depends on  $N_e$ , and it moves in the direction of the density minimum when  $N_e$  increases. The data are consistent with the model of an  $L_3$  exciton as consisting of a core having the charge  $2/3$  and a single split-off QE, as it was proposed by two of us previously.<sup>33</sup>

The dependence of the density distribution on  $h$  is shown in Fig. 9(b). This dependence is rather weak and is noticeable only in the vicinity of the hole. A large negative density near  $\theta = \pi$  is an artifact of the spherical model; it is unstable in this area [cf. Fig. 9(a)] and makes a small contribution to the total charge because of a small phase volume. A weak  $h$  dependence of  $d_L(r)$  in some areas of  $h$  values, and even exact absence of this dependence for nondegenerate states with small  $|\mathcal{M}|$  values, is typical of anyon excitons.<sup>49</sup>

The effect of the angular momentum  $L$  on the density distribution  $d_L(\theta)$  along the  $L_3$  branch is shown in Fig. 9(c). The changes in  $d_L(\theta)$  are dramatic. A narrow maximum appears near  $\theta = 0$  when  $L$  increases. It rapidly grows with  $L$ . As a result,  $d_L(\theta)$  curves acquire a three-maximum shape. For  $L = 5$  and  $6$  the charge about  $1/3$  is accumulated inside the low- $\theta$  maximum. As a result, an exciton comprises a narrow single-QE core and an extensive external two-peak shell. Such a picture resembles splitting anyons off from the central core with increasing  $k$  typical of anyon excitons.<sup>49</sup> Unfortunately, the size of the sphere is not sufficient for investigating the shape of the external shell in more detail.

In Fig. 9(d) the densities  $d_L(\theta)$  are shown for the  $L_3$  and  $L_5$  branches at their starting points ( $L = 3$  and  $5$ , respectively). As has been anticipated, the density distribution for  $L_5$  is wider and smoother than for  $L_3$ . For comparison, the density distribution for a single QE is also shown.

The symmetry arguments of Sec. VC show that  $L_3$  excitons are candidates for a description in terms of anyons. The data of Figs. 9(a), 9(c) are in reasonable agreement with this concept. Another important question is whether and under what conditions the anyon model can provide a consistent description of  $L_3$  excitons also on a *dynamic* level. If one accepts that the low- $\theta$  maximum in Fig. 9(c),  $L = 5$  and  $6$ , corresponds to a strongly bound QE, one should also conclude that its form factor is strongly squeezed as compared to a free QE, Fig. 9(d), by the attractive force of a hole. These data imply that the applicability region of the anyon picture of excitons is wider as applied to the symmetry classification of them than in description of their dynamic properties.

The electron density distribution for two excitons of

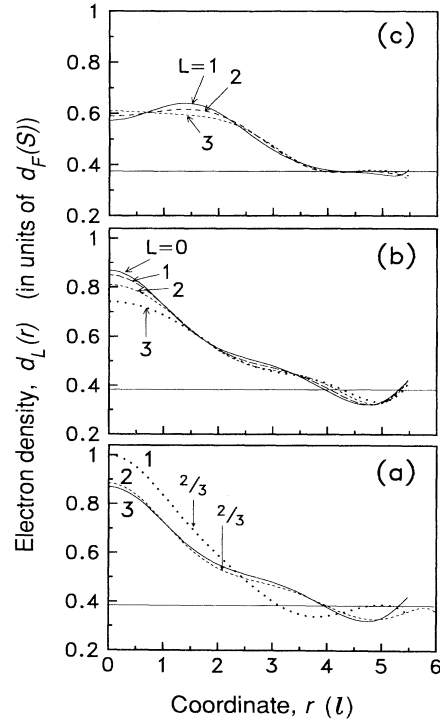


FIG. 10. Electron density distribution for  $L_0$  and  $L_1$  excitons. Data were obtained by averaging over  $L_z$ . (a) Density  $d_0(r)$  for an  $L_0$  exciton in the  $L = 0$  state. Data are shown for  $N_e = 7$ , and  $h = 0.6$  and  $2.6$  (curves 1 and 2, respectively), and for  $N_e = 8$ ,  $h = 2.6$  (curve 3). A good convergence of the data is seen. Arrows show the boundaries of the areas where a charge equal to  $2/3$  is accumulated. (b) Dependence of the density distribution  $d_L(r)$  on  $L$  for an  $L_0$  exciton;  $h = 2.6$ ,  $N_e = 7$ . (c) The same dependence for an  $L_1$  exciton;  $h = 2.6$ ,  $N_e = 7$ .  $h$  in units of  $l$ ,  $L$  in units of  $\hbar$ .

the second group,  $L_0$  and  $L_1$ , is shown in Fig. 10. For the  $L = 0$  state of an  $L_0$  exciton the density  $d_0(r)$  is close to the Fermi limit for  $r = 0$  and decreases rapidly with  $r$ , Fig. 10(a). It is natural that such a tight entity can not be described in terms of elementary excitations of a  $\nu = 1/3$  IQL. Weak oscillations in the density may be attributed to the oscillatory screening inherent in IQL's.<sup>60,61</sup> With increasing  $h$  a shoulder develops in the  $d_0(r)$  curve; the charge inside the core is close to  $2/3$ . This shoulder may indicate an increase in the projection of the wave function of the  $L_0$  exciton onto the low-energy sector with increasing  $h$ , cf. Sec. VC. The dependence of the density on  $L$  is shown in Fig. 10(b). It is slow and reveals no new features. The density distribution for an  $L_1$  exciton is shown in Fig. 10(c). It is narrow and depends on  $L$  but weakly. The deviation of the density from  $\nu = 1/3$  is moderate, about  $0.25$ .

Therefore two different groups of branches show absolutely different density distributions. For  $L_0$  and  $L_1$  the distributions are narrow, about two magnetic lengths, and weakly depend on  $L$ . In contrast,  $d_L(r)$  curves for  $L_3$  and  $L_5$  are considerably wider. For a  $L_3$  exciton the density shows a strong dependence on  $L$  and reveals features which can be treated in terms of split-off QE's. These

features are large as compared to those in the patterns of the oscillatory screening of  $L_0$  and  $L_1$  excitons, and the extra density has a constant sign nearly everywhere.

The spatial extension of  $L_3$  excitons is comparable with the sphere size even for the largest systems of  $N_e = 7$  and 8 electrons. The data for  $L_3$  excitons seem reliable, but the accuracy of the data for  $L_m$  excitons with  $m \geq 3$  should decrease with  $m$ . The fact that up to  $h = 3$  the  $L_3$  branch remains the lowest one and there are no branches which compete with it reflects the intrinsic restrictions of the spherical model.

## VI. SPHERE-ONTO-PLANE PROJECTION

The dynamic space of an exciton is a plane and not a sphere. Therefore, to facilitate developing a convenient description of excitons and find the selection rules for exciton transitions, it is necessary to establish a prescription for sphere-onto-plane projecting the exciton branches. In this section we establish the prescription and some spectroscopic consequences following from it.

### A. Generalized prescription

Exciton quantum numbers in the plane geometry are the projection  $M$  of the angular momentum of a  $k = 0$  exciton and the quasimomentum  $\mathbf{k}$ , while in the spherical geometry they are  $L_m$ ,  $L$ , and  $L_z$ . The quantum numbers  $M$  and  $L_m$  enumerate exciton branches, while  $\mathbf{k}$  and  $(L, L_z)$  describe the exciton states along the branches. The azimuth of  $\mathbf{k}$  and  $L_z$  form the spaces of degeneracy, while the energy along branches depends on  $k$  and  $L$ . Therefore the projection rule should relate  $L_m$  to  $M$  and  $L$  to  $k$ . For each branch we identify  $L_m$  as  $|M|$ , the modulus of the  $z$  projection of the angular momentum of the many-electron wave function. Since  $L_m$  is the minimum angular momentum for each branch, it is natural to consider it as the internal angular momentum ("spin") of an exciton.  $M$  is expected to differ from the angular momentum  $M$  of the corresponding Halperin's pseudo wave function<sup>6</sup> by the intrinsic angular momentum of a tight  $q$ -QE complex. This angular momentum can originate either from the relative angular momenta of composite fermions caused by the Pauli exclusion principle, or from orbital spins proposed in the modified<sup>62</sup> Landau-Ginzburg theory of IQL's.<sup>63</sup> Since all branches start at  $k = 0$  in the plane geometry, while at  $L_m$  in the spherical one, we identify  $L - L_m$  as  $kR$ :

$$L - L_m = kR. \quad (18)$$

Therefore the starting points  $L_m$  of all branches are identified with  $k = 0$ . Equation (18) generalizes the Haldane-Rezayi prescription<sup>9</sup>  $L = kR$  as applied to composite neutral quasiparticles bearing internal angular momenta  $L_m$ .

The quantum numbers discussed above are related to the symmetries. However, with increasing  $h$  and the sphere size  $R$  one should expect the appearance of several

branches with the same internal momentum  $L_m$ . Two well developed  $L_1$  branches are seen in the spectrum of an  $N_e = 8$ ,  $N_h = 1$  system, Fig. 11(a). They are designated as  $M_1$ 's since Fig. 11 is drawn in terms of the plane geometry.

The identification of  $L_m$  points as  $k = 0$  points imposes a strong restriction on the shape of exciton dispersion-law curves  $\varepsilon_m(L)$ . Since the  $k = 0$  point is a zero-slope point because of the time inversion symmetry, the slope of all  $L_m$  branches should decrease when  $L \rightarrow L_m$  (and turn into zero in the  $N_e \rightarrow \infty$  limit). Nearly all well developed  $\varepsilon_m(L)$  curves in Figs. 4 and 7 show this tendency. At the first glance, a considerable positive slope of the  $L_3$  branch at the point  $L = 3$ , Figs. 4(b), 4(c), and 7 (for an  $N_e = 7$ ,  $N_h = 1$  system), seems to contradict this expectation. However, a comparable negative slope of the  $L_3$  curve at the same point seen in Fig. 6 (for an  $N_e = 8$ ,  $N_h = 1$  system) indicates that the slope oscillates with  $N_e$ ; hence, a zero limit is quite natural for  $N_e \rightarrow \infty$ .

It is remarkable that the investigation of excitons (more generally, neutral elementary excitations) in a spherical geometry permits one to determine their angular momenta using only their dispersion laws  $\varepsilon(L)$ , without any additional information about their wave functions.

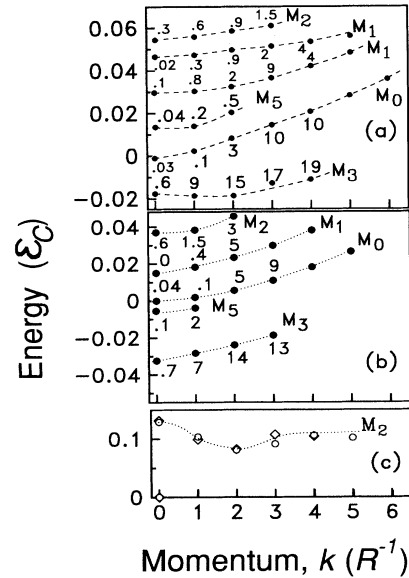


FIG. 11. Exciton and magnetoroton energy spectra, and probabilities of single-MR transitions. Energy spectra are plotted vs quasimomentum  $k$  according to the prescription of Eq. (18). (a), (b) Exciton energy spectra for systems of  $N_e = 8, N_h = 1, R = 3$  (a) and  $N_e = 7, N_h = 1, R = \sqrt{7.5}$  (b);  $h = 2.6$ . Numbers show transition probabilities (see the text for more detail), while  $M_m$  indicate  $|M|$  values. The probabilities are shown in percent of the transition probabilities from multiplicative states (for  $h = 0$ );  $h$  and  $R$  in units of  $l$ . (c) Energy spectrum of MR's for the systems of  $N_e^{(e)} = 6$  and 7, diamonds and dots, respectively. MR spectrum is plotted according to Eq. (18) for  $|M_{MR}| = 2$ .

### B. Selection rules and angular momentum of magnetorotons

Identification of the  $L = L_m$  points as  $k = 0$  points imposes rigorous restrictions on the selection rules for optical transitions. The selection rules for the direct transitions from the ground state are exactly the same in the both geometries; only the transition to the  $k = 0$  (or  $L = 0$ ) state of the  $M_0$  (or  $L_0$ ) branch is allowed.

The problem of selection rules is much more intricate and interesting as applied to indirect transitions which involve a single MR or some different neutral excitation of an IQL. Only a single selection rule, the conservation of the angular momentum  $L$ , exists in the spherical geometry. In contrast, in the plane geometry in addition to the  $k$  conservation law there exists also the  $M$  conservation law for  $k = 0$ . This means that most of the transitions to (from) the left ends of exciton branches,  $L = L_m$ , are artifacts of the spherical geometry and their intensities should disappear in the macroscopic limit,  $N_e \rightarrow \infty$ .

In Figs. 11(a) and 11(b) the energy spectrum  $\varepsilon_m(L)$  found in the spherical geometry is redrawn in the plane geometry according the generalized prescription of Eq. (18). Only well developed branches with an unambiguous assignment of at least two left-hand points are shown, and our usual restriction  $L \leq (L_{MR})_{\max}$  also is satisfied. For this reason  $L_4$ ,  $L_6$ , and  $L_7$  branches are omitted. The number by each point shows the optical transition probability. For  $L \neq 0$  the probability is shown for the transition to the lowest-energy state of the small system with the same value of  $L$ , i.e., for a single-MR assisted transition. For  $L = 0$  the probability of the transition to the first excited  $L = 0$  state of the small system is shown.  $M_m$  indicate exciton branches.

The classification of excitons by quantum numbers  $M$  and  $k$  implies that MR's which also are excitonlike (intra-Landau-level) excitations should possess the same quantum numbers,  $M_{MR}$  and  $k$ . Single-MR transitions at  $k = 0$  should be allowed only for exciton branches with  $M = M_{MR}$ . In contrast, for all exciton branches with  $M \neq M_{MR}$  the transition probability should vanish for  $k = 0$  (in the macroscopic limit) and show a fast increase with  $k$  in the small  $k$  region. It is seen from Figs. 11(a) and 11(b) that the branches  $M_3$ ,  $M_5$ ,  $M_0$ , and  $M_1$  show the behavior typical of forbidden transitions. For all these branches there is one order of magnitude difference in the probabilities for the first and the second points. Low transition probabilities at  $k = 0$  points and a reasonable agreement of the data found for  $N_e = 7$  and 8 indicate a satisfactory accuracy of the results. Low  $k = 0$  probabilities give an additional support to the generalized prescription of Eq. (18). The  $M_2$  branch seems to be the only candidate for allowed  $k = 0$  transitions. The probability shows much slower increase in the small  $k$  region as compared to different branches for both  $N_e = 7$  and 8. Meanwhile, the energy spectra differ strongly in the vicinity of  $M_2$  since the second  $M_1$  branch appears below  $M_2$  for  $N_e = 8$ . The persistent behavior of the  $M_2$  branch seems persuasive, and it suggests that the transition is weak but allowed. Therefore we propose that MR's of a  $\nu = 1/3$  IQL are  $|M| = 2$  excitations. Com-

putations in the spherical geometry do not specify the sign of  $M$ , but the analogy with the theory of anyon excitons<sup>49</sup> implies that  $M < 0$ ; hence,  $M_{MR} = -2$ .

The nature of MR's in the small  $L$  region had been a matter of discussion for a long time. The charge density excitation model<sup>10</sup> provides an excellent description of the MR's of a  $\nu = 1/3$  IQL near the roton minimum  $k_r$ , which corresponds to  $L=3-5$  depending on the number of electrons in the small system,  $N_e^{(s)}$ . However, it has been shown by computations<sup>64</sup> and analytical arguments<sup>65</sup> that the  $L = 1$  state is canceled by the usual projection procedure. This result is in complete agreement with the  $|M| = 2$  assignment of MR's. The nature of the  $L = 0$  state has attracted special attention. It has been proposed by Girvin *et al.*<sup>10</sup> that the  $L = 0$  state is a bound state of two MR's with momenta close to  $k_r$ , and this idea was supported by computational data.<sup>59</sup> The different nature of excitations with  $k \approx k_r$  and  $L = 0$  is in agreement with the above assignment of MR's since it implies that these excitations belong to two different branches, the former to the  $|M| = 2$  branch, while the latter to an  $M_0$  branch which has a higher energy and exists in some area of the  $k$  space near  $k = 0$ . However, it has been claimed recently<sup>66</sup> that the quasiexciton model<sup>11</sup> describes the energy levels of low-energy neutral excitations up to  $L = 1$ . These data, as well as the concepts of Ref. 62, favor the  $|M| = 1$  assignment. Although additional data are needed for resolving the controversy, it should be mentioned that the experimental observation<sup>35,36</sup> of Raman scattering by MR's supports the even- $M$  assignment of them. The  $|M| = 2$  assignment of MR's is also consistent with the polarization dependence of the Raman scattering found by Zang and Birman.<sup>38</sup> We feel that the most serious problem resulting from the  $|M| = 2$  assignment of MR's in conjunction with the prescription of Eq. (18) is a considerable decrease in the value of  $k_r$  below the value  $k_r \approx 1.4$  established by different approaches;<sup>4</sup> this problem needs a special consideration.

### VII. CONCLUSION

Investigation of the energy and optical spectra of a  $\nu = 1/3$  IQL as a function of the governing parameter  $h/l$  has revealed a spectacular development of the multiple-branch energy spectra for  $h/l \gtrsim 1.5$ .

If  $h/l \lesssim 1$ , the spectrum consists of a single exciton branch  $L_0$  and a quasicontinuum above it. The dispersion law  $\varepsilon_0(k)$  of the  $L_0$  branch becomes flatter when  $h/l$  increases. The wave functions of the exciton states show most considerable changes for the quasimomentum values about or larger than the quasimomentum  $k_r$  of the MR minimum,  $k \gtrsim k_r$ . These changes in wave functions result in the increase in the probabilities of single-MR transitions and, in conjunction with the renormalization of the exciton dispersion law, in the development in the emission spectra of doublets comprising the zero-MR and single-MR bands.

The most dramatic changes in the energy spectra are seen at  $h/l \gtrsim 1.5$  when new exciton branches split off from the bottom of the quasicontinuum, and the multiple-branch spectrum sets in. This spectrum con-

sists of branches of two types: anyon branches and tight excitons. They have a different origin and show a different behavior when  $h/l$  increases. Despite the fact that the number of electronic states increases with increasing system size, the exciton branches survive in the macroscopic limit, as well as their quantum numbers, mutual positions, electronic form factors, etc. Symmetry arguments based on the composite fermion formalism show that excitons belonging to these branches are compatible with the quasiatomic picture of neutral entities consisting of a valence hole of a charge  $(+e)$  and  $q$  anyons having charges  $(-e/q)$ . The energies of these branches drop down when  $h/l$  increases, and the branches find themselves below  $L_0$ . This behavior, as well as the electronic form factors of excitons and some other properties of them, are in agreement with the anyon model, at least as applied to the symmetry classification of them. All exciton branches of the anyon type are in one-to-one correspondence with definite states of the low-energy sector of the electron subsystem. This correspondence establishes a connection between excitons and the low-energy physics of IQL's. In contrast to anyon branches, tight excitons cannot be described in terms of the low-energy electronic excitations, and these branches remain above  $L_0$  at any  $h/l$  values.

A theory of composite fermions has been applied to the theory of hierarchies and to the behavior of quasiparticles in extended states in a number of papers. We have shown that composite fermions prove to be a useful tool for the symmetry classification of the bound states of several anyons.

The prescription for sphere-onto-plane projection, Eq. (18), sheds light on the physical meaning of the quantum numbers  $L_m$  labeling exciton branches. It identifies  $L_m$ 's as internal angular momenta of the excitons belonging to different branches. Therefore the prescription establishes a symmetry classification of the exciton branches. It should be applicable to different neutral excitations including intraband excitations.

The identification of  $L_m$ 's as internal angular momenta of excitons and  $(L - L_m)/R$  as their quasimomenta  $k$  establishes important selection rules for  $k = 0$  exciton transitions. Most of these selection rules exist in the real (plane) geometry but is absent in the spherical geometry.

In conjunction with the  $h/l$  dependence of the energies of different branches, these selection rules determine optical spectra of excitons. For example, the indirect transitions from the  $L_3, L_5$ , etc. anyon branches should dominate in the low- $T$  emission spectra at  $h/l \gtrsim 2$ , while direct transitions from the  $L_0$  branch should dominate at  $h/l \lesssim 2$ . When  $T \sim 10^{-2}\epsilon_C$ , which is a typical separation between different branches, the doublets comprising both direct and indirect bands should be seen. These patterns are robust, and the geometry of a heterojunction (quantum well) should mainly influence the critical value of  $h/l$ . In the low- $T$  absorption spectra direct transitions to the  $L_0$  band should dominate.

*Note added in proof.* Multiple-branch energy spectra of excitons have been also found and investigated in a recent paper by X. M. Chen and J. J. Quinn, Phys. Rev. B **51**, 5578 (1995). Two of us have shown that there exist drastic differences in the statistical properties of QE's and energy spectra of excitons of  $\nu = \frac{1}{3}$  and  $\nu = \frac{2}{3}$  IQL's. Data on the  $\nu = \frac{2}{3}$  IQL support the assignment of MR's as  $|M| = 2$  excitations [V. M. Apalkov and E. I. Rashba, Solid State Commun. **95**, 421 (1995)]. We have also mentioned that computations of F. D. M. Haldane [Phys. Rev. Lett. **55**, 2095 (1985)] performed for the square geometry with periodic boundary conditions resulted in the rotational angular momentum  $|\Delta M| = 2 \pmod{4}$  for the lowest  $\mathbf{k} = \mathbf{0}$  excited state; this result is in agreement with the  $|M| = 2$  assignment of MR's proposed above.

#### ACKNOWLEDGMENTS

We are grateful to Professor A. L. Efros for numerous fruitful and stimulating discussions. E.I.R. benefitted from suggestive discussions with Professor B. I. Halperin, Professor J. K. Jain, Professor D. E. Khmel'nitskii, Dr. P. M. Platzman, Professor E. H. Rezayi, and Professor T. M. Rice and is thankful to Professor R. G. Clark, Dr. D. Heiman, Dr. A. Pinczuk, and Professor A. Turberfield for explaining experimental data. The support by Subagreement No. KK3017 from QUEST of UCSB and by San Diego Supercomputer Center where the computations have been performed is acknowledged.

\* Present address: Department of Physics, University of California, Santa Barbara, CA 93106.

<sup>1</sup> R. B. Laughlin, Phys. Rev. Lett. **50**, 13 (1983).

<sup>2</sup> D. C. Tsui, H. Stormer, and A. C. Gossard, Phys. Rev. Lett. **48**, 1559 (1982).

<sup>3</sup> *The Quantum Hall Effect*, 2nd ed., edited by R. E. Prange and S. M. Girvin (Springer-Verlag, New York, 1990).

<sup>4</sup> T. Chakraborty and P. Pietiläinen, *The Fractional Quantum Hall Effect* (Springer-Verlag, New York, 1988).

<sup>5</sup> F. D. M. Haldane, Phys. Rev. Lett. **51**, 605 (1983).

<sup>6</sup> B. I. Halperin, Phys. Rev. Lett. **52**, 1583 (1984).

<sup>7</sup> J. K. Jain, Adv. Phys. **41**, 105 (1992).

<sup>8</sup> D. Arovas, J. R. Schrieffer, and F. Wilczek, Phys. Rev. Lett. **53**, 722 (1984).

<sup>9</sup> F. D. M. Haldane and E. H. Rezayi, Phys. Rev. Lett. **54**, 237 (1985).

<sup>10</sup> S. M. Girvin, A. H. MacDonald, and P. M. Platzman, Phys. Rev. **33**, 2481 (1986).

<sup>11</sup> R. B. Laughlin, Physica **126B**, 254 (1984).

<sup>12</sup> I. V. Kukushkin and V. B. Timofeev, Pis'ma Zh. Eksp. Teor. Fiz. **44**, 179 (1986) [JETP Lett. **44**, 228 (1986)]; I. Kukushkin, V. Timofeev, K. von Klitzing, and K. Ploog, Festkörperprobleme **28**, 21 (1988).

<sup>13</sup> V. M. Apalkov and E. I. Rashba, Pis'ma Zh. Eksp. Teor. Fiz. **53**, 420 (1991) [JETP Lett. **53**, 442 (1991)].

<sup>14</sup> B. I. Halperin, Helv. Phys. Acta **56**, 75 (1983).

<sup>15</sup> I. V. Kukushkin, R. J. Haug, K. von Klitzing, K. Eberl, and K. Töttemeyer, Phys. Rev. B **50**, 11 259 (1994).

<sup>16</sup> I. V. Kukushkin, R. J. Haug, K. von Klitzing, and K. Ploog, Phys. Rev. Lett. **72**, 736 (1994).

<sup>17</sup> D. Heiman, B. B. Goldberg, A. Pinczuk, C. W. Tu, A. C. Gossard, and J. H. English, Phys. Rev. Lett. **61**, 605

- (1988).
- <sup>18</sup> A. J. Turberfield, S. H. Heines, P. A. Wright, R. A. Ford, R. G. Clark, J. F. Ryan, J. J. Harris, and C. T. Foxon, *Phys. Rev. Lett.* **65**, 637 (1990).
  - <sup>19</sup> E. M. Goldis, S. A. Brown, R. B. Dunford, A. G. Davies, R. Newbury, R. G. Clark, P. E. Simmonds, J. J. Harris, and C. T. Foxon, *Phys. Rev. B* **46**, 7957 (1992).
  - <sup>20</sup> D. Z. Liu, H. A. Fertig, and S. Das Sarma, *Phys. Rev. B* **48**, 11 184 (1993).
  - <sup>21</sup> D. Heiman, A. Pinczuk, H. Okamura, M. Dahl, B. S. Dennis, L. N. Pfeiffer, and K. W. West, *Physica B* **201**, 315 (1994).
  - <sup>22</sup> T. V. Tatarinova, E. I. Rashba, and A. L. Efros, *Phys. Rev. B* **50**, 17 349 (1994).
  - <sup>23</sup> A. J. Turberfield, R. A. Ford, I. N. Harris, J. F. Ryan, C. T. Foxon, and J. J. Harris, *Phys. Rev. B* **47**, 4794 (1993).
  - <sup>24</sup> R. J. Clark, A. G. Davis, S. A. Brown, R. B. Dunford, P. E. Simmonds, A. C. Lindsay, R. Newbury, R. P. Starrett, A. Skougarevsky, E. E. Mitchell, R. P. Taylor, C. J. Mellor, B. L. Gallagher, C. T. Foxon, and J. J. Harris, *Physica B* **201**, 301 (1994).
  - <sup>25</sup> A. H. MacDonald, E. H. Rezayi, and D. Keller, *Phys. Rev. Lett.* **68**, 1939 (1992).
  - <sup>26</sup> V. M. Apalkov and E. I. Rashba, *Phys. Rev. B* **46**, 1628 (1992).
  - <sup>27</sup> E. H. Rezayi, in *Optical Phenomena in Semiconductor Structures of Reduced Dimensions*, edited by D. J. Lockwood and A. Pinczuk, Vol. 248 of *NATO Advanced Study Institute, Series E: Applied Sciences* (Kluwer, Dordrecht, 1993), p. 79.
  - <sup>28</sup> X. M. Chen and J. J. Quinn, *Phys. Rev. Lett.* **70**, 2129 (1993).
  - <sup>29</sup> E. I. Rashba and M. E. Portnoi, *Phys. Rev. Lett.* **70**, 3315 (1993).
  - <sup>30</sup> X. M. Chen and J. J. Quinn, *Phys. Rev. B* **50**, 2354 (1994).
  - <sup>31</sup> V. M. Apalkov and E. I. Rashba, *Phys. Rev. B* **48**, 18 312 (1993).
  - <sup>32</sup> A. H. MacDonald and E. H. Rezayi, *Phys. Rev. B* **42**, 3224 (1990).
  - <sup>33</sup> V. M. Apalkov and E. I. Rashba, *Pis'ma Zh. Eksp. Teor. Fiz.* **54**, 160 (1991) [*JETP Lett.* **54**, 155 (1991)]; **55**, 38 (1992) [**55**, 37 (1992)].
  - <sup>34</sup> V. M. Apalkov and E. I. Rashba, in *Conference Book of the 11th International Conference on High Magnetic Fields in Semiconductor Physics* (MIT, Cambridge, 1994), p. 278; E. I. Rashba and V. M. Apalkov, *ibid.*, p. 648; V. M. Apalkov and E. I. Rashba, *Solid State Commun.* **93**, 193 (1995). Unfortunately, there is a confusion in the scale of  $h$  values in these papers; all  $h$  values should be multiplied by the factor 2.
  - <sup>35</sup> A. Pinczuk, B. S. Dennis, L. N. Pfeiffer, and K. West, *Phys. Rev. Lett.* **70**, 3983 (1993).
  - <sup>36</sup> L. L. Sohn, A. Pinczuk, B. Dennis, L. N. Pfeiffer, K. West, and L. Brey, in *Conference Book of the 11th International Conference on High Magnetic Fields in Semiconductor Physics* (Ref. 34), p. 266.
  - <sup>37</sup> P. M. Platzman and S. He, *Phys. Rev. B* **49**, 13 674 (1994).
  - <sup>38</sup> J. Zang and J. L. Birman, *Phys. Rev. B* **51**, 5574 (1995).
  - <sup>39</sup> R. J. Elliott and R. Loudon, *J. Phys. Chem. Solids* **15**, 196 (1960).
  - <sup>40</sup> I. V. Lerner and Yu. E. Lozovik, *Zh. Eksp. Teor. Fiz.* **80**, 1488 (1981) [*Sov. Phys. JETP* **53** 763 (1981)].
  - <sup>41</sup> Yu. A. Bychkov, S. V. Iordanskii, and G. M. Eliashberg, *Pis'ma Zh. Eksp. Teor. Fiz.* **33**, 152 (1981) [*JETP Lett.* **33**, 143 (1981)].
  - <sup>42</sup> C. Kallin and B. I. Halperin, *Phys. Rev. B* **30**, 5655 (1984).
  - <sup>43</sup> L. P. Gor'kov and I. E. Dzyaloshinskii, *Zh. Eksp. Teor. Fiz.* **53**, 717 (1967) [*Sov. Phys. JETP* **26**, 449 (1968)].
  - <sup>44</sup> E. I. Rashba and V. M. Apalkov, in *Optical Phenomena in Semiconductor Structures of Reduced Dimensions* (Ref. 27), p. 63.
  - <sup>45</sup> Yu. A. Bychkov and E. I. Rashba, *Zh. Eksp. Teor. Fiz.* **85**, 1826 (1983) [*Sov. Phys. JETP* **58**, 1062 (1983)].
  - <sup>46</sup> D. Paquet, T. M. Rice, and K. Ueda, *Phys. Rev. B* **32**, 5208 (1985).
  - <sup>47</sup> A. B. Dzyubenko and Yu. E. Lozovik, *J. Phys. A* **24**, 415 (1991).
  - <sup>48</sup> E. I. Rashba and J. L. Birman, *Solid State Commun.* **84**, 99 (1992).
  - <sup>49</sup> M. E. Portnoi and E. I. Rashba, *Mod. Phys. Lett. B* **9**, 123 (1995).
  - <sup>50</sup> G. Fano, F. Ortolani, and E. Colombo, *Phys. Rev. B* **34**, 2670 (1986).
  - <sup>51</sup> F. G. M. Haldane, *Phys. Rev. Lett.* **67**, 937 (1991).
  - <sup>52</sup> S. He, X.-C. Xie, and F.-C. Zhang, *Phys. Rev. Lett.* **68**, 3460 (1992).
  - <sup>53</sup> M. K. Johnson and A. H. MacDonald, in *Physical Phenomena in High Magnetic Fields*, edited by E. Manousakis *et al.* (Addison-Wesley, Redwood, 1992), p. 102; M. K. Johnson and G. S. Canright, *Phys. Rev. B* **49**, 2947 (1994).
  - <sup>54</sup> B. N. Parlett and D. B. Scott, *Math. Comput.* **33**, 217 (1979).
  - <sup>55</sup> M. Crouzeix, B. Philippe, and M. Sadkane, *SIAM J. Sci. Comput.* **15**, 62 (1994); C. W. Murray, S. C. Racine, and E. R. Davidson, *J. Comput. Phys.* **103**, 382 (1992).
  - <sup>56</sup> F. C. Zhang and S. Das Sarma, *Phys. Rev. B* **33**, 2903 (1986).
  - <sup>57</sup> T. Ando, A. B. Fowler, and F. Stern, *Rev. Mod. Phys.* **54**, 437 (1982).
  - <sup>58</sup> G. Dev and J. K. Jain, *Phys. Rev. B* **45**, 1223 (1992).
  - <sup>59</sup> P. Béran and R. Morf, *Phys. Rev. B* **43**, 12 654 (1991).
  - <sup>60</sup> F. C. Zhang, V. Z. Vulovic, Y. Guo, and S. Das Sarma, *Phys. Rev. B* **32**, 6920 (1985).
  - <sup>61</sup> E. H. Rezayi and F. D. M. Haldane, *Phys. Rev. B* **32**, 6924 (1985).
  - <sup>62</sup> D.-H. Lee and X.-G. Wen, *Phys. Rev. B* **49**, 11 066 (1994).
  - <sup>63</sup> S. C. Zhang, T. H. Hansson, and S. Kivelson, *Phys. Rev. Lett.* **62**, 82 (1989).
  - <sup>64</sup> G. Dev and J. K. Jain, *Phys. Rev. Lett.* **69**, 2843 (1992); X. G. Wu and J. K. Jain, *Phys. Rev. B* **51**, 1752 (1995).
  - <sup>65</sup> S. He, S. H. Simon, and B. I. Halperin, *Phys. Rev. B* **50**, 1823 (1994).
  - <sup>66</sup> J. Yang, *Phys. Rev. B* **49**, 5443 (1994).